Journal of Materials Chemistry

Cite this: *J. Mater. Chem.*, 2012, **22**, 20358

www.rsc.org/materials

PAPER

Ce–surfactant lamellar assemblies with strong UV/visible emission and controlled nanostructures†

Takaaki Taniguchi,*[ab] Makoto Echikawa,[a] Yuki Naito,[a] Hikaru Tateishi,[a] Asami Funatsu,[a] Chikako Ogata,[a] Yukihiro Komatsubara,[c] Nobuhiro Matsushita,[c] Michio Koinuma[ab] and Yasumichi Matsumoto[ab]

Received 22nd May 2012, Accepted 9th August 2012
DOI: 10.1039/c2jm33265e

We describe self-organization–reorganization of a lanthanide (Ln)–surfactant lamellar hybrid with intense photoluminescence and controlled nanostructures. We reveal that UV luminescence exhibited by a Ce–dodecyl sulfate (DS) lamellar hybrid offers the maximum quantum yield (QY) of 90% among all types of Ce–organic hybrid materials. In addition, Ce–Tb dodecyl phosphate (DP) lamellar hybrids exhibit bright green emission due to the two-dimensional Ce^{3+}–Tb^{3+} energy transfer (ET) process in Ln–PO_4 layers. Furthermore, a Ce–DS film with a highly oriented nanostructure and Ce–Tb–DP colloidal nanosheets are fabricated through simple and effective reorganization routes. The concept of "reorganization routes" opens up new pathways to general- and large-scale fabrication of two-dimensional nanomaterials on the basis of metal–surfactant assemblies with a variety of physical and chemical properties.

Introduction

Self-assembly of amphipathic molecules has opened new routes to form beautiful one, two and three dimensional nano-architectures.[1,2] These assemblies have attracted increasing attention because of their potential applications in the wide fields of biochemistry and materials science. Hybridization of metal ions with surfactants is recognized as a new noncovalent interaction in the engineering of supramolecular assemblies with tunable physical and chemical properties.[3,4] Owing to their fascinating optical and magnetic properties, Ln^{3+} ions have been hybridized with various surfactants possessing carboxylate, sulfate, and phosphate moieties.[5,6] For example, it is widely accepted that the Ln ions and alkyl sulfate involving DS can self-organize tubular, lamellar, and hexagonal assemblies.[7–10]

Obtaining highly luminescent Ln surfactant assemblies is a simple but crucial research to further develop Ln surfactant hybrid materials; so far, no report is available regarding the presence of Ln surfactant assemblies with high quantum yields. In the case of a metal surfactant micelle complex, an OH ligand, a typical quenching agent, can strongly associate with the first coordination sphere of Ln ions to quench luminescence in an aqueous medium.[11] In contrast, it is hypothesized that Ln ions in a surfactant lamellar phase are passivated effectively by the surfactant moieties resulting in the minimization of nonradiative pathways induced by the OH vibrations. If such hybrid systems realize excellent luminescence with controlled nanostructures, their unique features involving low-temperature processes and high structural flexibility can be used in a variety of applications. These features, in addition to the high sensitivity to external fields[12] and stimuli,[3] are not exhibited by the conventional solid state phosphors.

In this context, we attempted to obtain highly luminescent lanthanide surfactant lamellar hybrids and succeeded in the synthesis of Ce–DS and Ce–Tb–DP lamellar hybrids with ultraintense UV and visible luminescence. Furthermore, we designed and demonstrated reorganization routes to the nanomaterials, developed on the basis of these highly luminescent lamellar hybrids; nanostructured thin films and nanosheets were fabricated *via* evaporation-induced self-assembly (EISA) and sonochemical exfoliation. The concept of "reorganization routes" opens up new pathways to general- and large-scale fabrication of two-dimensional nanomaterials exhibiting both functional properties and well-defined morphology controlled at the nanoscale.

Experimental

Synthesis of Ln–DS lamellar hybrid powder

Aqueous solutions of hydrated lanthanide nitrate (0.1 M) $La(NO_3)_3 \cdot 6H_2O$, $Ce(NO_3)_3 \cdot 6H_2O$, $Eu(NO_3)_3 \cdot 6H_2O$, $Tb(NO_3)_3 \cdot 6H_2O$,

[a]*Graduate School of Science and Technology, Kumamoto University, 2-39-1 Kurokami, Kumamoto 860-8555, Japan. E-mail: takatani@gpo.kumamoto-u.ac.jp*
[b]*JST, CREST, 7 gobancho, Chiyoda-ku, Tokyo 102-0075, Japan*
[c]*Materials and Structures Laboratory, Tokyo Institute of Technology, 4259 Nagatsuta, Midori-ku, Yokohama 226-8503, Japan*

† Electronic supplementary information (ESI) available: SEM images of La–DS and La–DP hybrids (Fig. S1). TEM images and XRD pattern of a La–DS lamellar hybrid (Fig. S2). XRD patterns of Ln–DS and Ln–DP lamellar hybrids (Fig. S4). PL spectra of Ln–DS and Ln–DP lamellar hybrids (Fig. S5). PL spectra of Ce–Tb–DS lamellar hybrids. See DOI: 10.1039/c2jm33265e

$Tm(NO_3)_3 \cdot 6H_2O$, $Pr(NO_3)_3 \cdot 6H_2O$, $Ho(NO_3)_3 \cdot 5H_2O$, and sodium dodecyl sulfate (SDS) (0.1 M, Wako, 99.5%) were prepared with Milli-Q water. 10 ml of lanthanide nitrate solution was added to a 30 ml SDS solution to precipitate an Ln–DS lamellar hybrid under ambient conditions. After the reaction, precipitates were collected by centrifugation, washed with distilled water, and dried at room temperature (RT) under vacuum.

Synthesis of Ln–DP lamellar hybrid powder

Aqueous solutions of hydrated lanthanide nitrate (0.1 M, Wako) and sodium dodecyl phosphate (SDP) (0.1 M, Tokyo Chemical Industry) were prepared with Milli-Q water. 10 ml of lanthanide nitrate solution was added to a 30 ml solution of SDP suspension, and the solution was stirred under ambient conditions overnight. After the reaction, precipitates were collected by centrifugation, washed with distilled water, and dried at RT under vacuum.

Fabrication of Ce–DS lamellar hybrid thin films by evaporation-induced self-assembly

0.01 g of Ce–DS lamellar hybrid powder was dissolved in 10 ml of ethanol. 5 μl of the solution was dropped onto a glass substrate, and then dried under ambient conditions.

Fabrication of 0.8Ce–0.2Tb–DP lamellar hybrid nanoparticles

0.1 g of 0.8Ce–0.2Tb–DP lamellar hybrid powder was dispersed in 30 ml of water, and the solution was treated ultrasonically. A stable colloid was obtained after centrifugation at 3000 rpm for 30 min to remove large particles.

Characterizations

Crystal structures were analyzed from XRD (Rigaku RINT-2500VHF) patterns obtained using Cu Kα radiation. PL spectra were obtained using a spectrofluorometer (Jasco FP-6500) with a 150 W Xe lamp at room temperature. Absolute QY was measured using a spectrofluorometer with an integrating sphere (Jasco ILF-533). The integration sphere allowed detection of excitation light reflected and scattered by a sample or $BaSO_4$ standard as well as photoluminescence from the sample, which enabled calculation of the ratio of the number of emitted photons to the number of absorbed photons (internal QY), and the ratio of the number of emitted photons to the number of irradiated photons (external QY). Excitation and emission spectra were calibrated for the spectral distribution of the Xe lamp intensity using rhodamine B (5.5 g l^{-1}, ethylene glycol solution) and a reference light source (Jasco ESC-333). TEM was performed with a Hitachi HF-2000 unit operating at 200 kV. Field emission scanning electron microscopy (SEM; Hitachi, SU-8000) was performed in a secondary electron imaging mode with an acceleration voltage of 5 kV. AFM was performed with a Nanocute (SII NanoTechnology Inc.) unit in tapping mode.

Results and discussion

Microplates based on Ln surfactant lamellar assemblies were obtained by one-pot reaction of SDS or SDP aqueous solution/dispersion with an $Ln(NO_3)_3$ aqueous solution (ESI, Fig. S1†). Fig. 1a and b show typical TEM images of the La–DP lamellar hybrid materials, presenting highly developed lamellar structures in which dark and light layers corresponded to inorganic and organic layers, respectively. The inter-lamellar distance was approximately 3–4 nm. The distance is close to that calculated from the XRD pattern, 3.5 nm (Fig. 1c). Such a nanoscale lamellar phase was confirmed for the La–DS hybrid (see ESI, Fig. S2†). The driving force that is used to form the lamellar architectures is based on the electrostatic attractive force between negatively charged surfactant moieties and positively charged Ln^{3+} ions, in addition to the hydrophobic interaction among alkyl-chains of the surfactants,[13] whereas the formation processes depend on the surfactant types. In the hybridization process of Ln with DS anions, it is accepted that Ln ions are precipitated with free DS^- anions and DS micelles to self-organize lamellar phases *via* a precipitation reaction.[14] On the other hand, SDP powder was not fully dissolved to form an aqueous dispersion. Therefore, the La–DP lamellar hybrid was formed *via* additional pathways to the precipitation reaction. We performed SEM-EDX analysis in order to describe the formation pathway to the La–DP hybrid (ESI, Fig. S3†). SEM and SEM-EDX elemental mapping images of a SDP sample show that microplates with an atomic ratio of Na/P of unity was formed in the aqueous dispersion before the reaction with La^{3+} ions. The overall plate-like shape remained after the reaction with La^{3+} ions, while EDX elemental mapping images show that P and La elements were distributed homogenously in the whole part of the products. The elemental analysis revealed that the La : P atomic ratio was close to 1 : 3, and Na was scarcely detectable after the reaction. Therefore, three Na^+ ions in vesicle multilayers could be exchanged with one La^{3+} ion in the lamellar phase to meet the charge compensation principle.

In our systematic investigation of the luminescent properties of a series of Ln–DS lamellar hybrids including Ln = La, Ce, Pr,

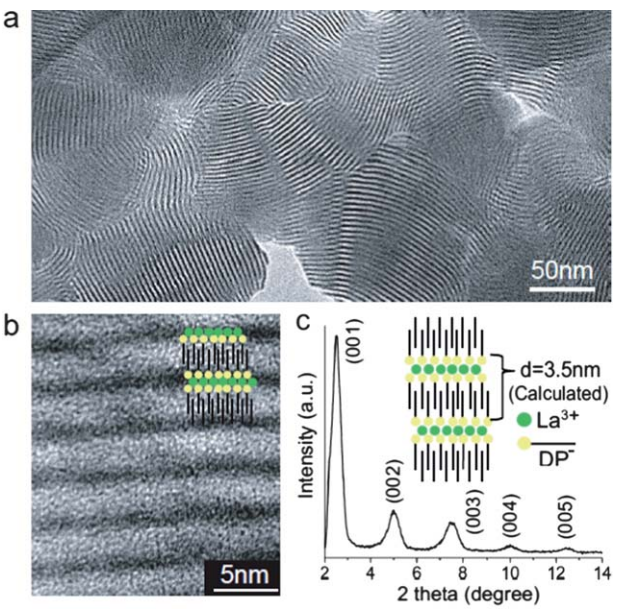

Fig. 1 (a) Low-magnification TEM image, (b) HRTEM image and (c) XRD pattern of La–DP.

Eu, Tb, Tm, and Ho (ESI, Fig. S4 and S5†), we observed that the Ce–DS lamellar hybrid exhibited ultraintense UV luminescence at *ca.* 320 nm (Fig. 2a). The photoluminescence (PL) emission spectra demonstrated that the luminescence was decomposed in two bands at 315 mm and 335 nm. This double peak luminescence suggests direct emission from the 2D ($5d_1$) state of Ce^{3+} to the two split $4f_1$ ground states of $^2F_{5/2}$ and $^2F_{7/2}$ caused by spin–orbit coupling.[15] The excitation spectrum monitored at 320 nm emission showed a band at approximately 284 nm that was attributed to the Ce^{3+} 4f → 5d transition. Note that La–DS and Na–DS lamellar hybrids gave no remarkable luminescent band in the UV-Vis range. Therefore, DS^- is inactive in luminescence, which excluded a contribution of "ligand to Ce^{3+} energy transfer" to the luminescence spectra. The lamellar hybrid offered a remarkably high QY_{int} (90%) of UV luminescence upon excitation at 280 nm. This value is the highest reported value to date, considering all types of available Ce–organic hybrids. This indicates that the relaxation process was nearly free from concentration quenching or quenching due to the presence of H_2O molecules. The strong PL in the Ce–DS lamellar hybrid contributed to the unique property of Ce^{3+}. Ce^{3+} emission occurred in the UV region, and the high corresponding energy prevented dissipation in the vibrations of water molecules. Nevertheless, many organic ligands have been discovered to quench Ce^{3+} luminescence upon complexation. Therefore, an interlayer space in the DS lamellar phase could provide a suitable environment for Ce^{3+} luminescence to minimize the nonradiative transition rate.

Investigation of the luminescent properties of a series of Ln–DP lamellar hybrids revealed that the Ce–DP lamellar hybrid

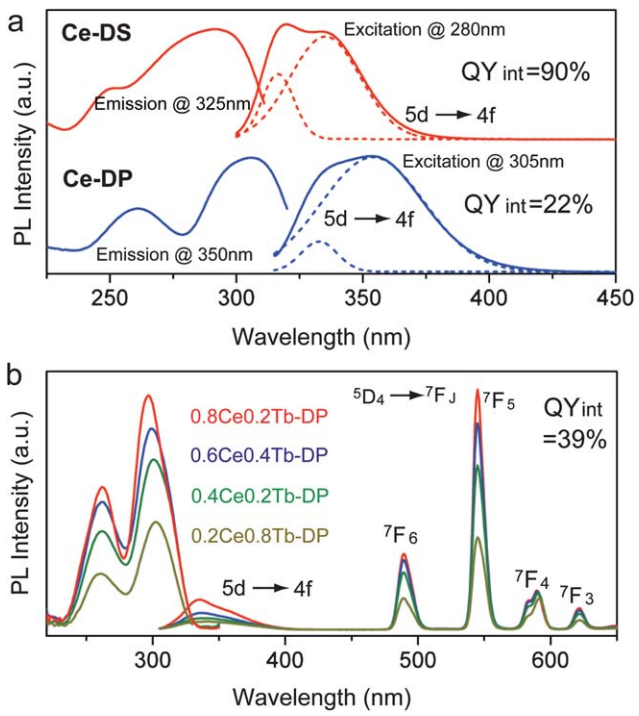

Fig. 2 (a) PL emission spectra and excitation spectra for Ce–DS and Ce–DP lamellar hybrids, and (b) PL emission spectra (excited at 300 nm) and excitation (monitored at 545 nm) spectra for $(1 - x)$Ce–xTb–DP lamellar hybrids.

offers the strongest luminescence (ESI, Fig. S4 and S5†). The luminescent spectra show double peaks located at 332 nm and 352 nm, respectively, due to the 5d–4f (Ce^{3+}) transitions (Fig. 2a),[15] and the QY_{int} of UV luminescence was 22% upon excitation at 295 nm. No luminescence was obtained for La–DP and Na–DP samples, which indicated the absence of the ligand to Ce^{3+} energy transfer in the emission process. We were able to obtain bright green luminescence in the Ce–Tb–DP binary lamellar phase. The emission spectra of the lamellar phase (Fig. 2b) consist of strong green emissions of the Tb^{3+} ions along with weak emissions of the Ce^{3+} ions. The emission lines from Tb^{3+} ions corresponded to four $^5D_4$ to ^7F_J ($J = 6$, 5, 4, and 3) transitions peaking at 488, 543, 584, and 619 nm, respectively.[16] The excitation spectrum monitored at 545 nm consisted mainly of the excitation bands of the Ce^{3+} ions, and was apparently different from that of Tb–DP hybrids (see ESI S5†), revealing that the Tb^{3+} ions were excited through the Ce^{3+} ions.[16] The 0.8Ce–0.2Tb–DP lamellar phase provided the highest intensity in the visible region with a QY_{int} of 39% among the samples. Furthermore, the external quantum yield (QY_{ext}) of the samples (29%) was significantly higher than that of the Tb–DP lamellar hybrids (1%), demonstrating that the intense luminescence was enabled by the high absorption coefficient of the Ce^{3+} (4f–5d) transition in addition to the high energy transfer and radiative transition rates. We note that the Ce–Tb–DS lamellar system showed a main UV luminescent band with relatively weak green emission bands from Tb^{3+}, which were similar to the Ce–Tb–DS micelle in aqueous solution[11] (ESI S6†). As shown before, Ce–DS exhibited a very high QY, which means that the lamellar structure was almost free from the concentration quenching process. This, in other words, can be interpreted to mean that the energy transfer process between Ce^{3+} ions was inactive. Therefore, it is possible to speculate that energy transfer from Ce^{3+} to Tb^{3+} is also inactive in the Ce–Tb–DS lamellar system. Such an efficient ET process between Ce^{3+} and Tb^{3+}, observed for Ce–Tb–DP hybrids, has been demonstrated for the first time in metal–organic hybrid materials, while the ET process has been reported in inorganic materials. $LnPO_4$ with a monazite phase is known to be a suitable host material for the activation of the Ce^{3+}–Tb^{3+} ET process.[16] We speculate that the Ce–Tb–DP lamellar hybrid locally exhibits –Ce–O–Tb– networks similar to those present in the $LnPO_4$ matrix so that the efficient ET process could take place in the two-dimensional layers. It is worth noting that Ln-based metal organic frameworks (MOFs) are attractive hybrid luminescent materials;[17] however, no report is available on MOFs with Ce^{3+}–Tb^{3+} ET, as organic building units prohibit ET in those cases. In contrast, metal ions are connected two-dimensionally through the moieties of surfactants in the metal–surfactant hybrid lamellar architecture so that, as we have demonstrated, the appropriate selection of surfactants can activate ET in the inorganic layers. This result can form a significant basis for designing functional metal surfactant lamellar phases based on heterometallic ions.

These results have demonstrated that organic ligands critically influence the luminescent properties of lamellar hybrids. In addition, chemical properties also depend on the surfactant species. In fact, we have discovered that the Ln–DS lamellar hybrid was dissociated to from a transparent solution in various organic solvents including methanol, ethanol, ethylene glycol,

and butanol, whereas Ln–DP powder was not soluble in any of these solvents or in water. We have used these features to demonstrate reorganization routes for the fabrication of nanostructured hybrid materials.

First, we demonstrate the fabrication of Ce–DS lamellar hybrid films by an EISA process.[18] In this method, first, the Ce–DS powder was dissolved in ethanol, second, the Ce–DS solution was dropped onto a glass substrate and finally, the solution was evaporated under ambient conditions (Fig. 3a). Fig. 3b and c show AFM images of the film fabricated with the EISA process and the corresponding cross-sectional profile, respectively, displaying the formation of a layered thin film with a flat surface and nanoscale steps in the microscale area. XRD revealed sharp (001) peaks (Fig. 3d) indicating that the lamellar crystal was oriented along the ⟨001⟩ direction on the glass substrate. The basal spacing calculated from the pattern (3.3 nm) was close to the minimum height of steps obtained in the cross-sectional profile, and the observed steps with 18.6 nm height approximately matched the thickness of six bilayers. PL data (Fig. 3e) indicate that the luminescent bands present on the film are similar to those observed in the initial Ce–DS powder. The data demonstrate that a Ce–DS lamellar hybrid film can be grown with a (001) preferential orientation on a glass substrate in an EISA process under ambient conditions. It is noted that the basal spacing of the lamellar film was 0.1 nm smaller than that of the initial powder (3.4 nm) (Fig. 3d), indicating that the superposition of alkyl chains in DS bilayers was larger and tilted more toward the inorganic layers, compared with that of the initial powder produced in an aqueous medium. Recently, Rauschenbach *et al.* have succeeded in ion-beam deposition of SDS films under vacuum conditions.[19] As an alternative deposition method, EISA is promising because of the simpler and greener deposition process in comparison with the vacuum process. Furthermore, we demonstrated that metal ions can be selectively intercalated between DS layers in the EISA route, which enable low-cost and large-scale fabrication of functional metal–surfactant hybrid films.

Colloidal Ce–Tb–DP nanosheets were obtained by a simple sonochemical top-down approach. It is known that the multilayer phospholipids can be exfoliated into bilayer or few layer vesicles *via* ultrasonic treatment. In fact, we yielded a stable aqueous colloidal suspension by a simple sonochemical top-down approach by ultrasonification using a conventional ultrasonic bath. AFM observation confirmed the presence of phospholipid bilayers with a thickness of *ca.* 3.5 nm (nanosheets) in the colloid (Fig. 4a). The nearly transparent colloidal solution exhibited bright green emission under irradiation at 254 nm with a UV lamp (Fig. 4b). The main excitation bands for 544 nm luminescence correspond to the 4f–5d excitation bands of Ce^{3+} ions (Fig. 4c), which indicates that the Ce and Tb ions were closely located at the surfaces of a bilayer vesicle, allowing energy transfer from Ce^{3+} to Tb^{3+}. The colloidal sample exhibits a QY_{int} of 6% at 320 nm excitation. The decrease in luminescent efficiency after the exfoliation process is due to the nonradiative pathways induced by OH groups associated with Ln^{3+} spices at vesicle surfaces. Recently, exfoliation of layered materials involving graphene oxides,[20] oxides,[21–24] hydroxides,[25,26] sulfates,[27,28] and MOFs[29] has been intensively investigated to obtain functional nanosheets. For

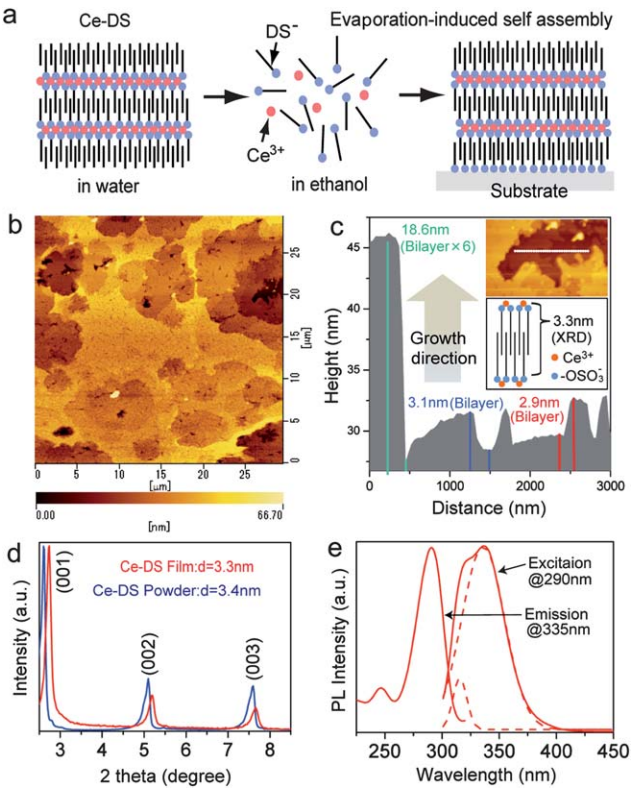

Fig. 3 (a) Schematic illustration of an EISA reorganization route to the Ce–DS lamellar hybrid film. (b) AFM image of a Ce–DS lamellar hybrid film grown by EISA. (c) Cross-sectional AFM profile. XRD patterns of a Ce–DS film grown by ESIA and Ce–DS powder. (d) PL emission PL emission spectra and excitation spectra for a Ce–DS film grown by EISA.

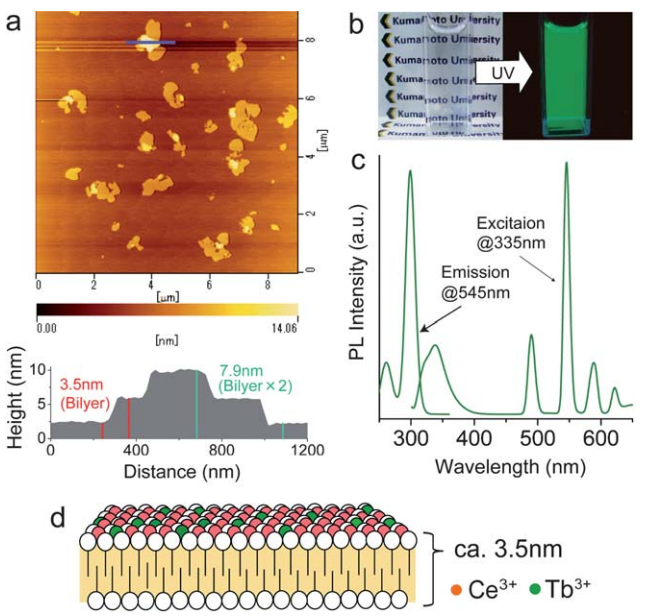

Fig. 4 (a) AFM image and cross-sectional profile of 0.8Ce–0.2–DP nanosheets exfoliated by ultrasonic treatment in water. (b) Photograph of 0.8Ce–0.2Tb–DP nanosheets aqueous dispersion with/without UV light irradiation. (c) PL emission spectra and excitation spectra for 0.8Ce–0.2Tb–DP nanosheets. (d) Schematic illustration of a Ce–Tb–DP vesicle nanosheet.

example, we developed Ln-based luminescent inorganic nanosheets such as $Gd_{1.4}Eu_{0.6}Ti_3O_{10}$, $La_{0.7}Tb_{0.3}Ta_2O_7$ and $Bi_xSr_{1-x}Ta_2O_7$.[22,30] In this study, we succeeded in the fabrication of luminescent metal–surfactant hybrid nanosheets for the first time. Ce-based two-dimensional nanophosphors allow chemical switching of $Ce^{3+} \leftrightarrow Ce^{4+}$ to tune the luminescent properties.[31] In addition, phospholipids are expected to have membrane properties such as storage, transport, and separation abilities. Along with the luminescent properties and high dispersability in aqueous medium, these features make the hybrid nanosheets attractive for biomedical/chemical applications.

Conclusion

In conclusion, we have developed highly luminescent Ln–surfactant lamellar hybrids and reorganization processes. The Ce–DS lamellar hybrid exhibited strong UV luminescence with a maximum QY_{int} of 90%. The Ce–Tb–DP binary lamellar hybrids allow two-dimensional Ce–Tb ET to produce bright green emission. These highly emitting phosphors reorganized *via* EISA and sonochemical exfoliation methods to form highly oriented hybrid films and vesicle nanosheets, respectively. These reorganization routes can be applied to various metal–surfactant assemblies in principle. Therefore, the concept opens simple-, general-, and large-scale routes to two-dimensional nanomaterials with a variety of chemical and physical properties. In our ongoing work, we have investigated magnetic and catalytic properties of reorganized lanthanide–surfactant nanohybrids, and also explored reorganization routes to transition metal–surfactant assemblies with controlled properties and nanostructures.

Acknowledgements

This work was supported by the Core Research of Evolutional Science & Technology (CREST) of the Japan Science and Technology Agency, Grant-in-Aid for Young Scientists(B) (no. 23710131), and Grant-in-Aid for Scientific Research(A) (no. 23245036).

Notes and references

1 T. Kunitake, *Angew. Chem., Int. Ed. Engl.*, 1992, **31**, 709–726.
2 T. Shimizu, M. Masuda and H. Minamikawa, *Chem. Rev.*, 2005, **105**, 1401–1443.
3 K. Kuroiwa, M. Yoshida, S. Masaoka, K. Kaneko, K. Sakai and N. Kimizuka, *Angew. Chem., Int. Ed.*, 2012, **51**, 656–659.
4 H. Matsukizono, K. Kuroiwa and N. Kimizuka, *J. Am. Chem. Soc.*, 2008, **130**, 5622–5623.
5 N. M. Selivanova, A. I. Galeeva, A. T. Gubaydullin, V. S. Lobkov and Y. G. Galyametdinov, *J. Phys. Chem. B*, 2012, **116**, 735–742.
6 K. Behera and S. Pandey, *J. Colloid Interface Sci.*, 2007, **316**, 803–814.
7 M. Yada, S. Sakai, T. Torikai, T. Watari, S. Furuta and H. Katsuki, *Adv. Mater.*, 2004, **16**, 1222–1226.
8 M. Yada, M. Mihara, S. Mouri, M. Kuroki and T. Kijima, *Adv. Mater.*, 2002, **14**, 309–313.
9 A. J. M. Valente, H. D. Burrows, S. M. A. Cruz, R. F. P. Pereira, A. C. F. Ribeiro and V. M. M. Lobo, *J. Colloid Interface Sci.*, 2008, **323**, 141–145.
10 A. J. M. Valente, H. D. Burrows, R. F. Pereira, A. C. F. Ribeiro, J. L. G. C. Pereira and V. M. M. Lobo, *Langmuir*, 2006, **22**, 5625–5629.
11 M. J. Tapia, H. D. Burrows, M. E. D. G. Azenha, M. Da Graça Miguel, A. A. C. C. Pais and J. M. G. Sarraguça, *J. Phys. Chem. B*, 2002, **106**, 6966–6972.
12 D. Yan, J. Lu, J. Ma, S. Qin, M. Wei, D. G. Evans and X. Duan, *Angew. Chem., Int. Ed.*, 2011, **50**, 7037–7040.
13 R. F. P. Pereira, M. J. Tapia, A. J. M. Valente and H. D. Burrows, *Langmuir*, 2012, **28**, 168–177.
14 R. F. P. Pereira, M. J. Tapia, A. J. M. Valente, R. C. Evans, H. D. Burrows and R. A. Carvalho, *J. Colloid Interface Sci.*, 2011, **354**, 670–676.
15 B. F. Aull and H. P. Jenssen, *Phys. Rev. B*, 1986, **34**, 6647–6655.
16 V. Buissette, M. Moreau, T. Gacoin, J. P. Boilot, J. Y. Chane-Ching and T. Le Mercier, *Chem. Mater.*, 2004, **16**, 3767–3773.
17 J. Rocha, L. D. Carlos, F. A. A. Paz and D. Ananias, *Chem. Soc. Rev.*, 2011, **40**, 926–940.
18 C. J. Brinker, Y. Lu, A. Sellinger and H. Fan, *Adv. Mater.*, 1999, **11**, 579–585.
19 S. Rauschenbach, G. Rinke, N. Malinowski, R. Weitz, R. Dinnebier, N. Thontasen, Z. Deng, T. Lutz, P. M. de Almeida Rollo, G. Costantini, L. Harnau and K. Kern, *Adv. Mater.*, 2012, **24**, 2761–2767.
20 S. Stankovich, D. A. Dikin, R. D. Piner, K. A. Kohlhaas, A. Kleinhammes, Y. Jia, Y. Wu, S. T. Nguyen and R. S. Ruoff, *Carbon*, 2007, **45**, 1558–1565.
21 K. Fukuda, Y. Ebina, T. Shibata, T. Aizawa, I. Nakai and T. Sasaki, *J. Am. Chem. Soc.*, 2007, **129**, 202–209.
22 S. Ida, C. Ogata, M. Eguchi, W. J. Youngblood, T. E. Mallouk and Y. Matsumoto, *J. Am. Chem. Soc.*, 2008, **130**, 7052–7059.
23 Y. Omomo, T. Sasaki, L. Wang and M. Watanabe, *J. Am. Chem. Soc.*, 2003, **125**, 3568–3575.
24 M. Choi, K. Na, J. Kim, Y. Sakamoto, O. Terasaki and R. Ryoo, *Nature*, 2009, **461**, 246–249.
25 S. Ida, D. Shiga, M. Koinuma and Y. Matsumoto, *J. Am. Chem. Soc.*, 2008, **130**, 14038–14039.
26 R. Ma, Z. Liu, K. Takada, N. Iyi, Y. Bando and T. Sasaki, *J. Am. Chem. Soc.*, 2007, **129**, 5257–5263.
27 J. N. Coleman, M. Lotya, A. O'Neill, S. D. Bergin, P. J. King, U. Khan, K. Young, A. Gaucher, S. De, R. J. Smith, I. V. Shvets, S. K. Arora, G. Stanton, H. Y. Kim, K. Lee, G. T. Kim, G. S. Duesberg, T. Hallam, J. J. Boland, J. J. Wang, J. F. Donegan, J. C. Grunlan, G. Moriarty, A. Shmeliov, R. J. Nicholls, J. M. Perkins, E. M. Grieveson, K. Theuwissen, D. W. McComb, P. D. Nellist and V. Nicolosi, *Science*, 2011, **331**, 568–571.
28 C. Schliehe, B. H. Juarez, M. Pelletier, S. Jander, D. Greshnykh, M. Nagel, A. Meyer, S. Foerster, A. Kornowski, C. Klinke and H. Weller, *Science*, 2010, **329**, 550–553.
29 J. C. Tan, P. J. Saines, E. G. Bithell and A. K. Cheetham, *ACS Nano*, 2012, **6**, 615–621.
30 S. Ida, C. Ogata, U. Unal, K. Izawa, T. Inoue, O. Altuntasoglu and Y. Matsumoto, *J. Am. Chem. Soc.*, 2007, **129**, 8956–8957.
31 Y. Xiang, X. F. Yu, D. F. He, Z. Sun, Z. Cao and Q. Q. Wang, *Adv. Funct. Mater.*, 2011, **21**, 4388–4396.

